Annu. Rev. Phys. Chem. 2001. 52:165–92


# COINCIDENCE SPECTROSCOPY

Robert E Continetti
*Department of Chemistry and Biochemistry, University of California at San Diego, La Jolla, California 92093–0314; e-mail: rcontinetti@ucsd.edu*

**Key Words** reaction dynamics, dissociative photodetachment, dissociative photoionization, molecular-frame photoelectron angular distributions, three-body dissociation

■ **Abstract** The application of coincidence techniques to the study of the reaction dynamics of isolated molecules is reviewed. Coincidence spectroscopy is a powerful approach for carrying out a number of measurements. At its most basic level, coincidence techniques can identify the source of a specific signal, as in the well-known photoelectron-photoion coincidence approach used for several years. By carrying out coincidence experiments in an increasingly differential manner, correlated energy and angular distributions of reaction products may be recorded. Completely energy- and angle-resolved measurements of photoelectrons and ionic or neutral products can reveal molecular-frame photoelectron and photofragment angular distributions and aid in the characterization of dissociative states of molecules and ions. Recent work in this area is reviewed, including examples from studies of dissociative photodetachment, dissociative photoionization, time-resolved studies of dissociative photoionization, and three-body dissociation processes.

## INTRODUCTION

The reaction dynamics of transient molecules and clusters is an area of gas-phase physical chemistry with significant fundamental questions that remain to be answered. The dissociative and metastable electronic states involved in photoexcitation processes, as well as the transition state region of the potential energy surface that governs the outcome of bimolecular reactions, have not been characterized as well as the bound states of molecular systems because of a lack of appropriate experimental tools. Studies of the dynamics of unimolecular dissociations and bimolecular reactions are one approach to probing these states. Over the last 30 years, photodissociation and bimolecular reactions have been examined in increasing detail using laser and molecular beam techniques (1, 2). However, the need for further experimental information has continued to drive the development of new experimental techniques for the study of transient species.

Even though the theoretical machinery of quantum chemistry is well developed, there are still important limitations in our ability to calculate the properties

0066-426X/01/0601-0165$14.00 

of electronically excited and dissociative states of stable molecules and the ground-state properties of transient species such as free radicals, anions, and weakly bound clusters (3, 4). Quantum mechanical methods in reaction dynamics are even more limited; accurate quantum mechanical calculations without dynamical approximations remain limited to systems of four or fewer atoms (5). To continue to drive these fields forward, new and refined experimental observables on dissociative electronic states, ionization processes, and the reaction dynamics of small molecules and clusters are required. The development of coincidence spectroscopies has arisen in part because of this need.

Coincidence spectroscopies can provide important information, unavailable from conventional spectroscopic techniques, regarding the identity and energetics of reactive species, the correlation of product states, the nature of repulsive electronic states, and insights into product angular distributions in the molecular frame. Coincidence techniques are also providing important insights into three-body dissociation processes, an area in which little information beyond rate coefficients has been available in the past. This review focuses on some of the recent applications of coincidence spectroscopies to the energetics and reaction dynamics of isolated molecules and clusters.

Coincidence techniques were originally developed to aid in the identification of the source of specific signals, as in the well-known photoelectron-photoion coincidence (PEPICO) approach used for several years (6). PEPICO experiments have been continually improved in many ways, ranging from the measurement of threshold photoelectrons (7) to recent fully energy- and angle-resolved experiments. This review focuses on the latter experiments in which individual correlated events are accumulated one at a time with subsequent analysis of the correlations contained therein. Thus, this review does not touch on the important contributions made by imaging techniques, wherein correlated properties of reaction products can be measured by spectroscopic state selection (e.g. multiphoton ionization) followed by measurement of product translational energy and angular distributions using charge-coupled-device (CCD)-based detection schemes. These applications were recently reviewed (8–11).

## Energetic Correlations

Two types of observables from coincidence experiments are highlighted here: (*a*) the use of energetic correlations to characterize dissociative molecular electronic states and the transition state region of bimolecular reactions and (*b*) the use of angular correlations between photoelectrons and photofragments—and also among multiple photofragments—to characterize the ionization and dissociation dynamics. The energetic correlations involve examination of the photoelectron kinetic energy distribution and how it correlates with different product channels in a molecular dissociation. For either photoionization of neutral molecules or photodetachment of negative ions, the interpretation of these energetic correlations is very similar: The photoelectron kinetic energy distribution contains information about the Franck-Condon overlap between the initial bound state and the metastable

or repulsive state that is reached by photoexcitation. The photofragment translational energy distribution, on the other hand, contains information about how the system prepared in the Franck-Condon region couples to the dissociation continuum. In the simplest case of no energy transfer among the products during the dissociation, then, the product translational energy distribution reveals the energetic repulsion between the products relative to the dissociation asymptote (12). Examples of the application of these energetic correlations to understanding dissociative photodetachment (DPD) and dissociative photoionization (DPI) processes and the potential energy surface near the transition state for bimolecular reactions are discussed below.

## Molecular-Frame Photoelectron Angular Distributions

An important quantity that can be measured in a coincidence experiment is the molecular-frame photoelectron angular distribution (MF-PAD). It is well known that the laboratory photoelectron angular distribution (PAD) recorded in photoionization or photodetachment of a randomly oriented sample with linearly polarized light is as follows (13):

$$\frac{\partial\sigma}{\partial\Omega_{\mathrm{LAB}}} = \frac{\sigma_{\mathrm{total}}}{4\pi}\left[1 + \beta(E)P_2(\cos\theta)\right], \qquad 1.$$

where $\sigma_{\mathrm{total}}$ is the total photodetachment cross section, $\theta$ is the polar angle between the recoil direction and the electric vector of the laser, and $P_2(\cos\theta)$ is the second-order Legendre polynomial in $\cos\theta$. The energy-dependent asymmetry parameter $\beta(E)$ is a sensitive function of both the symmetry of the orbital from which the electron is removed and the photodetachment dynamics. However, owing to the averaging over molecular orientations in the measurement of a laboratory angular distribution, detailed information on the partial-wave composition of the ionization continuum is lost. Measurement of MF-PADs, however, provides considerably more information. As Dill (14) showed, the MF-PAD is given by

$$\frac{\partial\sigma(E)}{\partial\Omega_{\mathrm{MF}}} = \sum_{l=0}^{2l^*}\sum_{m} A_{\mathrm{lm}}(E)\,Y_{\mathrm{lm}}(\vartheta,\varphi), \qquad 2.$$

where $l^*$ is the maximum value for the orbital angular momentum of the photodetached electron and $m$ corresponds to the azimuthal quantum number for the photodetached electron. The magnitudes of the energy-dependent coefficients $A_{\mathrm{lm}}(E)$ are determined by electric-dipole selection rules and interference between the degenerate photoelectron continuum channels. These coefficients thus contain detailed information on both the photodetachment dynamics and the orbital from which the electron is ejected, determining the relative contributions of the spherical harmonics $Y_{\mathrm{lm}}$, which are referenced to the molecular frame by the polar and azimuthal angles $\vartheta$ and $\varphi$.

A number of studies of MF-PADs have focused on the use of aligned molecular ensembles produced by photoexcitation (15). However, DPI or DPD processes

provide an alternative approach to studying fixed-in-space molecules. When dissociation is rapid relative to molecular rotation (axial recoil) (16), measurement of the recoil angle of the photoelectron relative to the axis of the broken bond in the molecule provides a direct measure of the MF-PAD in a coincidence experiment. Experiments on both DPD and DPI that are sensitive to the MF-PAD are reviewed below.

Photoelectron spectroscopy has also been applied to time-resolved studies of reaction dynamics (17, 18). Because photoelectron spectra are sensitive to changes in the electronic structure as a chemical reaction, isomerization, or nonradiative transition proceeds, femtosecond time-resolved photoelectron kinetic energy spectra have revealed important insights into nonadiabatic processes (19–21) and solvation phenomena (22). As mentioned in the last paragraph, although, PADs and in particular MF-PADs are the most sensitive probes of the electronic structure and ionization dynamics, so there has been an increasing interest in time-resolved studies of these observables. Theoretical efforts include the development of methods for the prediction and analysis of time-resolved PADs and MF-PADs in molecular photoionization (23–28). Experimentally, time-resolved laboratory PADs have been measured (20, 29), and recently studies of MF-PADs have been extended into the femtosecond time domain in the fully energy- and angle-resolved PEPICO experiments on the DPI of $NO_2$ by Davies et al (30, 31), as reviewed below.

## Three-Body Dissociation Dynamics

Coincidence experiments are also well suited to the study of three-body dissociation dynamics. Important insights into both concerted and sequential dissociation reactions have been gained from noncoincident studies of three-body photodissociation processes (32, 33). However, general techniques to perform the coincidence measurements required to directly measure product angular correlations in neutral molecules were not available until the recent DPD experiments in our group (34) and charge-exchange/laser-excitation experiments by Helm and coworkers (35). These experiments join earlier studies of the three-body dissociation dynamics of multiply charged ions (36–38) in revealing three-dimensional product momenta. Such measurements allow the investigation of not only the partitioning of energy in three-body dissociation processes, but also a second important molecular-frame quantity: the angular correlation of the momenta of the three atomic or molecular fragments. We refer to this quantity as the molecular-frame differential cross section (MF-DCS), which gives immediate insights into the dynamics, including the dissociation lifetime and molecular geometry at the instant of dissociation. In particular, if the three-body dissociation is rapid (the axial recoil approximation mentioned above, although the choice of axis in the three-body dissociation is system-dependent), this is a direct molecular-frame measurement, sensitive to both the molecular structure and dissociation dynamics of the system in question.

Recent examples of coincidence studies of DPD, DPI, and three-body dissociation dynamics are discussed below. First, a brief review of experimental techniques is presented.

## EXPERIMENTAL TECHNIQUES

Recent progress in the area of coincidence spectroscopy has been enabled by developments in both detection technology and the increased availability of new light sources, including synchrotrons and laboratory laser systems with kilohertz repetition rates. The experiments discussed in this review are all coincidence measurements of the three-dimensional velocity distributions of the atomic, molecular, or photoelectron products of a dissociation event. To carry out a coincidence measurement successfully, several factors must be considered. The product collection efficiency must be sufficiently high and the sources of background sufficiently small that a valid correlation between observed events can be made. In addition, these experiments must be carried out under conditions of relatively low signal rates and high duty cycles to overcome the problems associated with finite detection efficiencies (12, 39). In this review, two applications of coincidence spectroscopy are discussed: photoionization of neutral molecules in a molecular beam and fast ion-beam experiments involving photodetachment of negative ions or charge-exchange neutralization of cations.

The first priority in setting up a coincidence experiment is to ensure that the products can be detected with a high efficiency. If the products are charged, as in a photoionization process that will produce a free electron and a photoion, extraction with an appropriate field allows collection of all the products. In a DPI process, for example, producing a free electron, a photoion, and a photoneutral, measurement of the time- and position-of-arrival of the charged products (electron and ion) at a detector provides the information required for a complete kinematic description of the dynamics. This is the approach taken in the energy- and angle-resolved PEPICO experiments reviewed here. Takahashi and coworkers (40), for example, recently described an imaging PEPICO spectrometer that uses opposed time- and position-sensitive detectors to record the two-dimensional projection of the three-dimensional velocity distribution. With short-pulse laser or synchrotron radiation and time- and position-sensitive detectors with 0.1-ns timing resolution, a similar opposed detector geometry has been used to directly record the three-dimensional velocity distributions of both photoelectrons and photoions in coincidence. This technique has been used in DPI studies (41–43), including the recent time-resolved experiments of Hayden and coworkers (30).

If the products are neutral, the detection problem is more challenging. The simplest approach to carrying out coincidence studies involving neutral products is the use of fast (keV) ion beams followed by photodetachment (in the case of anions), charge exchange neutralization (in the case of cations), or collision-induced dissociation. Fast ion beams have the important property of allowing efficient ($\sim$50%) detection of neutral products with laboratory energies in excess of 1 keV upon impact with a microchannel-plate-based detector (44). In addition, in a fast beam, the products are constrained by momentum conservation to a limited angular range in the laboratory frame because of the high beam velocity. This situation allows the full solid angle in the center-of-mass (CM) frame to be covered with a single detector, similar to the techniques for charged particles discussed above.

The fast-beam method coupled with time- and position-sensitive particle detection was pioneered by DeBruijn & Los (45) in studies of the dissociative charge exchange of diatomic molecules. Measurement of the time and position of particle arrival, coupled with the knowledge of the parent mass and velocity, allows determination of the product mass ratio, scattering angles, and CM translational energy release ($E_T$) in the dissociation. In contrast to studies of ions, where the product mass can be determined with high accuracy by time-of-flight mass spectrometry, in a fast-beam experiment, the product mass ratio is determined by momentum conservation in the CM frame. The finite size of the parent beam typically limits the mass resolution to $m/\Delta m \approx 15$ (12). The low mass resolution is a challenge when the branching ratio between several open channels must be determined in the dissociation of a polyatomic molecule. In three-body dissociation experiments where all the products are detected, the time and positions of impact give the product velocities and recoil angles in the CM frame. Identification of the products requires some chemical intuition concerning the possible dissociation channels. Then, given the conservation of mass and momentum in the CM frame, the mass of each of the products can be determined (34). The error in determining product masses in three-body dissociation is more significant, with $m/\Delta m \approx 2.5$.

Fast-beam coincidence spectroscopies have several applications, including the dissociative charge exchange of diatomic (46) and polyatomic molecules (47, 48), photodissociation processes of cations (49), and neutral species generated by photodetachment (50, 51). It is beyond the scope of this review to cover these two-body dissociation processes in detail. The restriction here will be to processes that produce three or more products, including DPD: $ABC^- + h\nu \rightarrow A + BC + e^-$ and higher-order processes.

Coincidence studies of DPD require detection of the energy and angle of recoil of each photoelectron produced. In a fast ion beam, detection has occurred in two ways. The first approach involves large, solid-angle, short-flight-path time-of-flight photoelectron detectors with detection efficiencies from 2 to 10% of all photoelectrons (34, 52). These spectrometers require subnanosecond lasers since the photoelectron flight time for electron-volt-range photoelectrons may be only 50–100 ns. The time and position of electron impact is used to determine the actual flight distance for the photoelectron, angle of recoil, and laboratory energy. By knowing the velocity of the negative ion beam, the laboratory energy of the photoelectron can be corrected to give the CM photoelectron kinetic energy, *eKE*. With this approach, an energy resolution of $\Delta E_{FWHM}/E \sim 5\%$ (where FWHM is full width at half maximum) can be achieved routinely.

A second approach is to extract the photoelectrons with a small electric field in a space-focusing time-of-flight configuration, as was previously applied to photoionization processes (30). In this configuration, timing resolution becomes critical, as the range of photoelectron flight times for forward and backward scattered electrons (relative to the detector) may be <10 ns. In fast-beam experiments in our laboratory, we have achieved an energy resolution of $\Delta E_{FWHM}/E \sim 12\%$ with this

approach. We recently reported on photodetachment imaging in a fast-negative-ion beam study of the electron affinity of $CF_3$ (53).

Studies of three-body dissociation processes producing neutral products in fast beams face the special challenge that all three products strike the particle detector typically within a few hundred nanoseconds. Thus, the detection technique must be carefully chosen. In fast-beam processes producing two fragments, for example, two individual detectors can be used, such as the coincidence wedge-and-strip anode configuration used by Continetti et al (50), which uses charge division on a patterned anode (54), an approach that is limited for multiparticle applications by the several microseconds of dead time per particle. In 1992, Brenot & Durup-Ferguson (55) discussed the various experimental techniques available for multiparticle time- and position-sensitive detection, and several technological approaches to this problem have resulted from studies of molecular structure by Coulomb explosion techniques (56, 57).

There is an increasing use of hybrid techniques involving CCD-based detectors for imaging, which are coupled with less dense discrete-anode photomultiplier tubes for acquiring timing information. This type of detector has been used by Amitay et al (58) in dissociative recombination studies and will likely see further application in coincidence experiments, in particular as the readout rate for CCD cameras continues to increase. In addition, several groups have begun to use crossed-delay line anodes for recording time- and position-of-impact data (34, 59, 60). Delay line methods have an inherent advantage over charge division techniques because they use fast timing signals to determine the position of impact. With fast timing signals, fast logic and switching techniques can be used to set up multihit encoding electronics. This approach has been taken in developing the quadrant crossed-delay-line anode in our laboratory for the study of three-body dynamics (34). This device can record the time and position of arrival of up to eight particles arriving within 10 ns if they are spread out over the detector correctly. This redundancy in detection provides a nearly ideal three-body detector, although some kinematic configurations remain difficult to study in a single experiment.

## COINCIDENCE STUDIES OF DISSOCIATIVE PHOTODETACHMENT

### Energy and Angular Correlations: $O_4^-$

Coincidence studies of DPD processes provide a novel way to probe both photodetachment dynamics and the properties of the dissociative states of transient neutral molecules. As discussed above, these experiments are based on the production of mass-selected negative-ion beams, photodetachment, and recording the kinetic energies and recoil angles of the photoelectron and any photofragments produced after dissociation of the nascent neutral species.

Coincidence studies of DPD dynamics build on the important studies of photodetachment of stable negative ions that correspond to unstable neutral species (61–65). The photoelectron spectra in these cases can be analyzed to gain insights into a neutral potential energy surface that is unstable with respect to isomerization or dissociation. Analysis of these spectra constitutes a spectroscopy of the transition state. The photoelectron spectra provide information on the Franck-Condon overlap between the bound anion and the dissociative or unstable region of the neutral potential energy surface. When the nascent neutral species undergoes dissociation, insights into the potential energy surface for bimolecular reactions can be gained, as shown for example by the studies of Neumark and coworkers (62) on the hydrogen exchange reactions X + HY, where X and Y are F, Cl, Br, or I (62), and by studies of the fundamental F + $H_2$ reaction (63). This approach has also been used by Lineberger and coworkers (61) to study isomerization processes such as conformational changes in cyclooctatetraene. These photodetachment studies have stimulated theoretical studies interpreting the observed photoelectron spectra in terms of the potential energy surfaces and the scattering dynamics for these fundamental reactions (66, 67).

For DPD, however, a more complete coincidence measurement is required to fully characterize both the Franck-Condon region (from the photoelectron spectrum) and the ensuing dissociation dynamics (from the product translational energy distribution). In the photoelectron-photofragment coincidence (PPC) experiments developed in our laboratory, complete kinematic characterization of two- and three-body DPD processes is achieved by detection of the photoelectron in coincidence with the atomic or molecular products (34, 68, 69). Determination of the energies and recoil angles of all products allows determination of the correlated photoelectron-photofragment kinetic energy release and MF-PADs for photodetachment, as shown in studies of $O_4^-$ (70). These experiments have recently been extended to three-body dissociation dynamics, as discussed below. Here, the DPD dynamics of $O_4^-$ and our recent study of the transition-state dynamics of the OH + $H_2O \rightarrow H_2O$ + OH reaction (71) are reviewed.

As an example of the application of PPC spectroscopy to the study of DPD, consider the case of $O_4^-$:

$$O_4^- + h\nu \rightarrow O_2\left(^3\Sigma_g^-\right) + O_2\left(^3\Sigma_g^-\right) + e^-. \qquad 3.$$

$O_4^-$ is essentially an oxygen dimer bound together by a delocalized electron, with a dissociation energy of 0.46 eV (72). Photodetachment of the anion produces two $O_2$ molecules in close proximity, with approximately 0.4 eV of repulsive energy. Dissociation occurs on the time scale of molecular vibration. This is an example of a direct DPD process. The experimental signature of these dynamics can be seen most clearly in the work we carried out on this system at 532 nm (2.33 eV) (69, 70). The energetic correlations in a system like this can be displayed in the form of a two-dimensional photoelectron-photofragment correlation spectrum, $N(E_T, eKE)$. This spectrum shows the number of events with specific $E_T$ and e*KE* as a contour map,

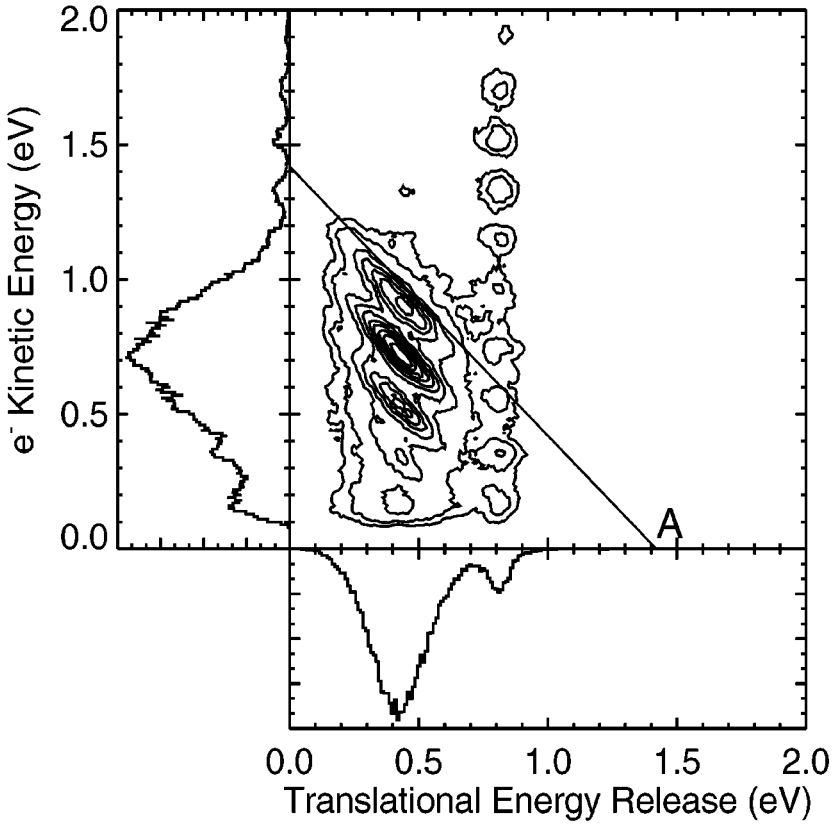


**Figure 1** $N(E_T, eKE)$ correlation spectrum for $O_4^-$ recorded at 532 nm shown as a contour plot of the energy partitioning in dissociative photodetachment. The one-dimensional $N(E_T)$ and $N(eKE)$ spectra are shown along the $x$ and $y$ axes, respectively. The maximum kinetic energy for photodetachment to $O_2(X, v = 0) + O_2(X, v = 0) + e^-$ is shown as limit $A$. The diagonal features correspond to DPD to different correlated $O_2$ product vibrational states, for example, ($v = 0, v = 0$), ($v = 0, v = 1$), etc (adapted from Reference 70 with permission from Elsevier Science).

as shown in Figure 1. The photoelectron and photofragment translational energy spectra obtainable in noncoincidence experiments are shown alongside the appropriate axes in this figure and represent integration of the coincidence spectrum over the complementary variable. The photoelectron spectrum, dominated by a broad peak at 0.7 eV, reproduces that originally obtained by Johnson and coworkers (73). Fine structure observed at higher kinetic energies is a result of the photodissociation of $O_4^-$: $O_4^- + h\nu \rightarrow O_2(^1\Delta_g) + O_2^-(^2\Pi_g)$, followed by photodetachment of the $O_2^-$ product by a second photon. The translational energy spectrum is dominated by a broad peak at 0.4 eV, with a smaller narrow peak at 0.8 eV.

The correlation observed between these one-dimensional distributions is striking: A series of diagonal lines is observed despite the lack of structure in either the photoelectron or translational-energy spectra. This is an example of a system exhibiting vibrationally adiabatic dissociation dynamics on a repulsive surface under conditions in which little rotational excitation is possible in the dissociation. Because of the steepness of the repulsive neutral surface, photodetachment to the various vibrationally adiabatic final states overlaps considerably in the photoelectron spectrum. Nonetheless, due to constrained exit channel dynamics, with no exchange of vibrational energy and limited rotational excitation, clearly resolved diagonal lines are observed in the correlation spectrum. Another way to view this is in terms of a spectrum of the total translational energy release, $N(E_{\mathrm{TOT}})$, where $E_{\mathrm{TOT}} = \mathrm{e}KE + E_{\mathrm{T}}$ summed for each event. This spectrum is shown in Figure 2, which reveals a well-resolved spectrum with peaks spaced by $O_2$ product vibrations (70). The spacings of the first five vibrational levels of $O_2$ are shown as combs on the spectrum for reference. Structural information on gas-phase $O_4^-$ can be obtained from this spectrum.

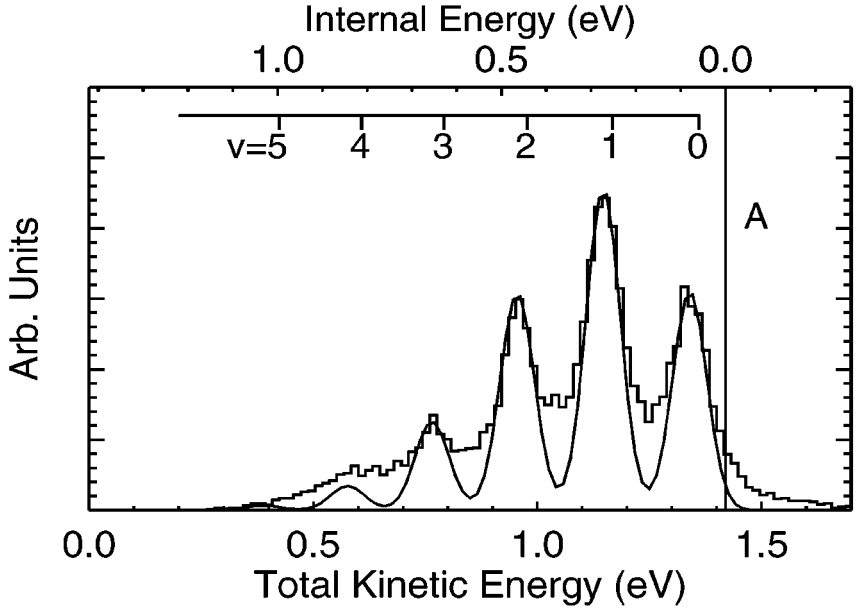


**Figure 2** $N(E_{\mathrm{TOT}})$ spectrum for the dissociative photodetachment of $O_4^-$ at 532 nm. The energetic limit is the same as that shown in Figure 1. The top axis indicates the internal energy, and the bottom axis shows the total translational energy ($\mathrm{e}KE + E_{\mathrm{T}}$). The data are represented by points, and the solid-line fit to the data was generated by a Franck-Condon simulation assuming two $O_2$ subunits with equal O–O bond lengths of 1.272 Å (adapted from Reference 69 with permission from the American Physical Society).

A simple simulation was performed by calculating the Franck-Condon overlap of the vibrational wave functions of two perturbed $O_2$ molecules with two free ground-state $O_2$ molecules. The results of this calculation are plotted as a solid line in Figure 2, and it was found that assuming equal bond lengths of 1.272 Å gave excellent agreement with the data. This result indicates that the excess electron is delocalized over the two $O_2$ moieties in a symmetric structure, consistent with recent ab initio calculations by Aquino et al (74).

The dynamics observed in the DPD of $O_4^-$ at 532 nm provide an example of what will occur in a direct DPD with a constrained product state distribution. Photodetachment occurs to a repulsive state of the neutral surface, and the time scale of the dissociation of the neutral fragments is a function of the steepness of the repulsive surface accessed by photodetachment. In Reference 70, application of a bound-free Franck–Condon formalism to analysis of the repulsive states of $O_4$ was made.

Other limiting cases of DPD dynamics as observed by PPC spectroscopy can be established by considering the time scale for photodetachment and the subsequent dissociation of the neutral complex. A second limiting case is sequential DPD, where the electron departs and then later the neutral system dissociates, either by predissociation or unimolecular decomposition on the electronic ground state. In this case, resolved vibrational structure may be observed in the photoelectron spectrum, and the dissociation dynamics of specific vibronic states of the neutral complex may be determined in the coincidence experiment. The best example of this type of process, with sharp structure in the photoelectron spectrum and no diagonal structure observed in the correlation spectrum, is the DPD of $O_3^-$ (75). In this case, predissociation of the initial relatively long-lived vibronic states produced by photodetachment gives rise to horizontal structure along the $E_T$ axis in the correlation spectrum. As these techniques are extended to polyatomic systems, there is no guarantee that these limiting dynamics can be identified, owing to the larger number of internal degrees of freedom. An example of this situation is the DPD process $N_3O_2^- + h\nu \rightarrow NO + N_2O + e^-$ (76). The correlation spectrum for this system shows no structure other than that dictated by energy conservation. This system may not behave vibrationally adiabatically in DPD, or rotational excitation in the exit channel, and the limited energy resolution of the experiment may prevent observation of structure in the correlation spectrum.

Finally, in PPC experiments, the angular correlations between the photoelectrons and photofragments can also be recorded. For a direct DPD, such as $O_4^-$, the direction of recoil of the $O_2$ products provides a record of the distribution of $O_4^-$ anions in the laboratory that absorbed photons. Because the $O_2$ photoproducts were found to have a highly anisotropic angular distribution, and the photoelectrons from photodetachment of $O_4^-$ are also anisotropically distributed in space (77), the angular correlations between the photoelectrons and photofragments were examined for evidence of an anisotropic MF-PAD. In these experiments, the photoelectron detector subtended only 4% of the total solid angle, so the presence of an anisotropic MF-PAD can be identified by examining events in which an electron

and two $O_2$ products are detected and comparing the observed $O_2$ photofragment angular distribution with that found from events with only two $O_2$ products detected. Detection of the photoelectron in coincidence, in a direction nearly orthogonal to the electric vector of the laser, breaks the cylindrical symmetry around the electric vector of the laser in the laboratory frame. This observation was reported in References 69 and 70. In these experiments, the $O_2$ photofragment angular distribution is nearly $\sin^2\theta$ at 532 nm. Examining only those events coincident with detection of a photoelectron showed a pronounced reduction of $O_2 + O_2$ photofragment recoils detected parallel to the direction of photoelectron detection. The existence of this angular correlation shows that photodetachment and dissociation of the nuclear framework of $O_4$ both occur on a time scale that is fast relative to molecular rotation (~1–10 ps) and that the photoelectron preferentially recoils perpendicularly to the dissociation coordinate in $O_4$.

The evidence for a strong anisotropy of the MF-PAD implies that a limited number of electron partial waves contribute in the detachment process. Electronic structure calculations on $O_4^-$ by Aquino et al (74) have shown that $O_4^-$ has $D_{2h}$ symmetry with a $^2A_u$ electronic ground state. Application of symmetry considerations, as discussed by Brauman and coworkers (78), indicates that d-wave photodetachment is expected near the threshold for this system (70). This conclusion also can be reached by qualitative consideration of the $a_u$ highest occupied molecular orbital (HOMO) for $O_4^-$. This HOMO has three angular nodes and is thus analogous to an atomic *f* orbital, resulting in both *d*-wave ($l = 2$) and *g*-wave ($l = 4$) photodetachment following the atomic selection rules of $\Delta l = \pm 1$ (79). Above threshold, however, the higher-angular-momentum states of the photoelectron continuum are accessible and will lead to an energy-dependent PAD, which has been observed in experiments at 355 and 266 nm (70). Now that detailed electronic structure calculations on $O_4^-$ have become available (74), a more detailed interpretation of the photodetachment dynamics in this interesting anion, using electron-molecule scattering calculations, should be possible.

## Transition-State Dynamics: $OH + H_2O \rightarrow H_2O + OH$

The thermoneutral identity reaction $OH + H_2O \rightarrow H_2O + OH$ is one of the simplest hydrogen abstraction reactions involving the hydroxyl radical and provides an excellent case for studying transition-state dynamics by DPD. The groundwork for this study was laid by the photoelectron studies of Arnold et al (65) of the $H_3O_2^-$ anion. They observed a broad photoelectron spectrum with at least four identifiable peaks at 266 nm (4.66 eV). The spectrum was observed to undergo significant changes, in both intensities and positions, upon deuteration, implying that the spectral features were primarily related to motion of the hydrogen atoms in the complex. They also carried out ab initio calculations and one-dimensional Franck-Condon simulations of the spectrum, confirming the role played by motion of the transferred H atom in the neutral $OH(H_2O)$ complex produced by photodetachment.

The transition-state dynamics of this reaction have been studied using DPD of $OH^-(H_2O)$ and $OD^-(D_2O)$ at 258 nm (4.80 eV) using PPC spectroscopy (71).

DPD is the only process that occurs at this photon energy:

$$OH^-(H_2O) + h\nu \rightarrow OH + H_2O + e^-. \quad 4.$$

The quantum yield for dissociation of the neutral complex into two fragments is unity. No stable $OH(H_2O)$ clusters are produced because the geometry of the anion leads to no Franck-Condon overlap with the $OH(H_2O)$ van der Waals geometry. The photoelectron spectra are consistent with the previous results of Neumark and coworkers (65). The PPC spectrum for the $OH^-(H_2O)$ anion, however, reveals considerably more information.

The correlation of the broad peaks in the electron kinetic energy spectrum (*eKE*) and photofragment translational energy release ($E_T$) for $OH^-(H_2O)$ reveals a series of four diagonal ridges (shown in Figure 3). As shown in Reference 71, the $OD^-(D_2O)$ anion gives analogous results, with five features observed owing to the lower stretching frequencies in the deuterated neutral complex. The previous observations on $O_4^-$ suggest that DPD onto vibrationally adiabatic curves in the repulsive region near the transition state for the neutral bimolecular reaction, correlating with the different asymmetric-stretch vibrational states of the $H_2O$ products, is responsible for these features. This assignment cannot be made on energetic grounds alone, however, because the asymmetric stretch of $H_2O$ and the stretching frequency of OH are nearly degenerate. Quantum chemical calculations on the anion and the neutral complex indicate that in the H–O–H–O–H structure the exterior O–H bonds are nearly at the equilibrium value, so it is expected that the product OH will be vibrationally cold, with excitation of the asymmetric stretch of the water that received the shared H atom (71).

As discussed above for $O_4^-$, examination of the total translational energy spectra $N(E_{TOT})$ is another informative way to view the $N(E_T, eKE)$ correlation spectra. In the $N(E_{TOT})$ spectra for the $H_3O_2^-$ and $D_3O_2^-$ systems shown in Figure 4, the diagonal features in the correlation spectra appear as a resolved spectrum of the correlated product vibrational distribution. Examination of the offset of the vibrational peaks from the internal energy origin (dissociation asymptote) shows that rotational and bending excitation in the products is small. Compared with the photoelectron spectra, the $N(E_{TOT})$ spectra show more structure and a nicely resolved progression in both the nondeuterated and deuterated case. The observed peak spacing of ~0.42 eV (3390 $cm^{-1}$) in $H_3O_2^-$ and ~0.33 eV (2660 $cm^{-1}$) in $D_3O_2^-$ is consistent with the interpretation of excitation of the antisymmetric stretch vibration in the water product.

Some further comments on the nature of the $N(E_{TOT})$ spectra and how they differ from the photoelectron spectra should be made. The spacing and width of the peaks in a photoelectron spectrum are determined by the Franck-Condon overlap between the stable anion and the dissociative neutral surface. The lifetime broadening effects of a steeply sloped repulsive surface yield broad features in the photoelectron spectrum. The translational energy release, $E_T$, between the atomic or molecular products in DPD is governed by both the region of Franck-Condon overlap with the neutral surface and any subsequent transfer of energy from internal

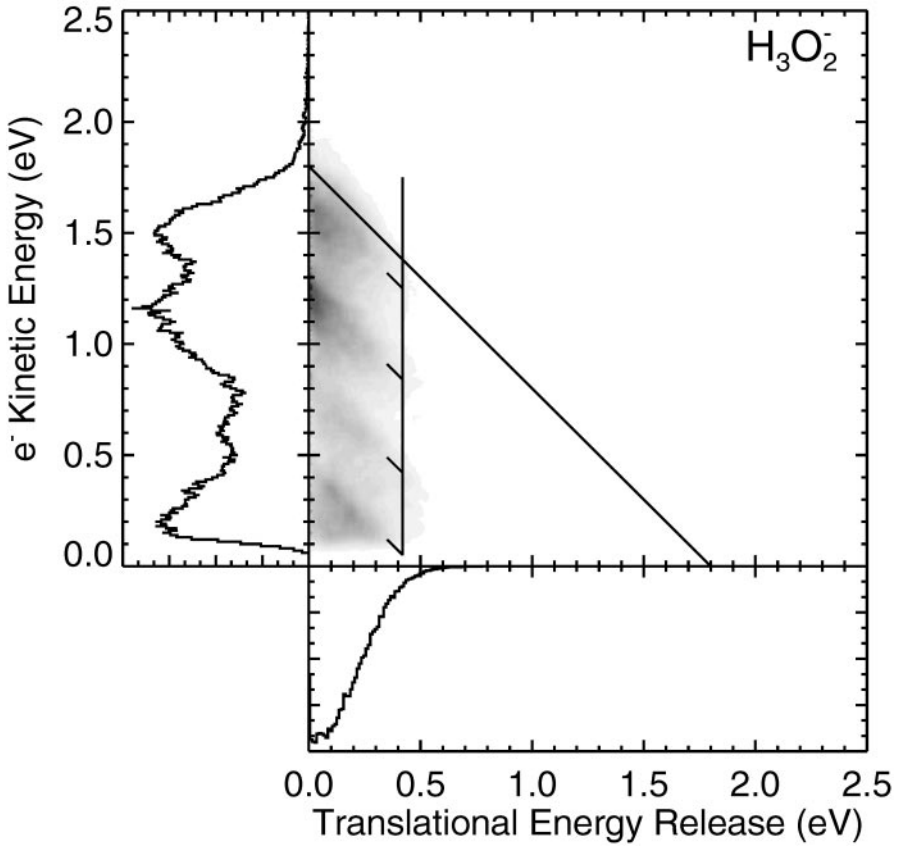


**Figure 3** Photoelectron-photofragment energy correlation spectrum [$N(E_T, eKE)$] represented as a two-dimensional gray-scale histogram for $H_3O_2^- + h\nu \rightarrow H_2O + OH + e^-$ at 258 nm. The comb shows the asymmetric-stretch spacing of the $H_2O$ product, and the maximum energy available is shown by the diagonal line (reproduced by permission of the Royal Society of Chemistry from Reference 71).

to external degrees of freedom in the dissociation, as discussed in the introduction. The total translational energy release, $E_{TOT} = eKE + E_T$, however, is determined solely by energy conservation. Thus, in the case of $H_3O_2^-$, $E_{TOT} = E_{h\nu} - D^0(OH^- - H_2O) - EA(OH) - E_{int}[OH(i) + H_2O(j)]$. Here, $D^0(OH^- - H_2O)$ is the bond dissociation energy of $H_3O_2^- \rightarrow OH^- + H_2O$, $EA(OH)$ is the adiabatic electron affinity of OH, and $E_{int}$ is the sum of the internal energy of states $i$ and $j$ in the products. Irrespective of the exit channel dynamics, the partitioning of $E_{TOT}$ into e$KE$ and the sum $E_T + E_{int}$ is determined by the bound-free Franck-Condon overlap between the anion and neutral surface. The $N(E_{TOT})$ spectrum is a direct, resolved measure of the product internal state distribution

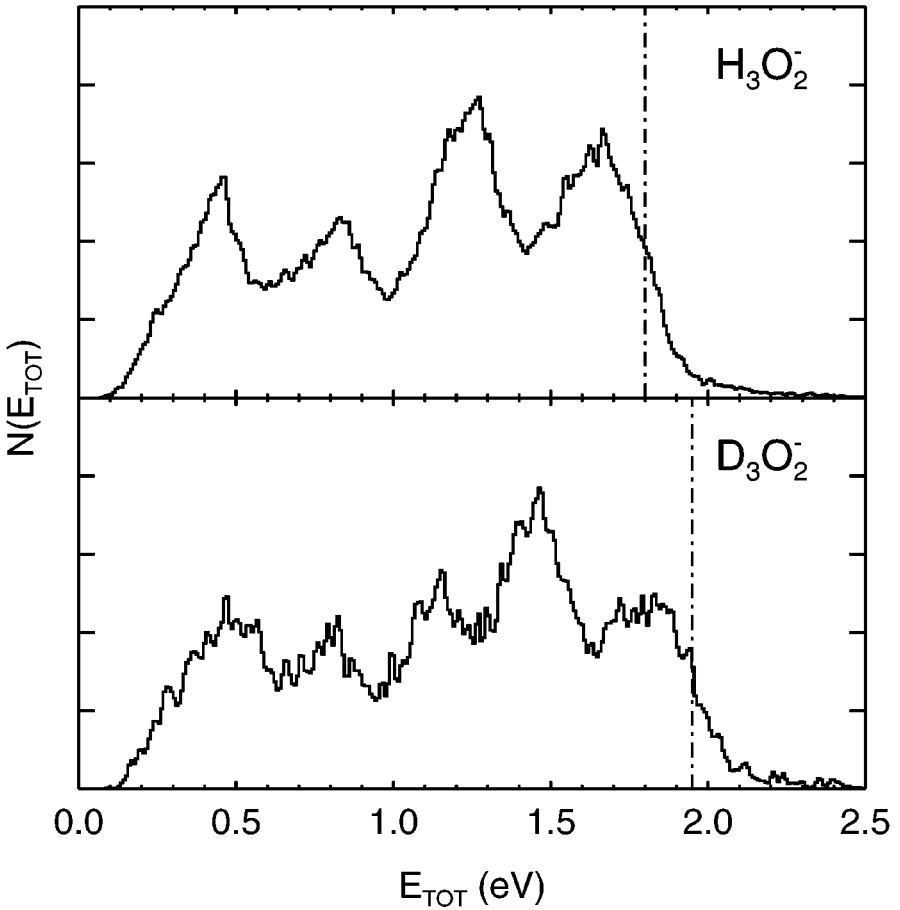


**Figure 4** Vibrationally resolved product translational energy [$N(E_{TOT})$] spectra for the dissociative photodetachment (DPD) of $H_3O_2^-$ and $D_3O_2^-$ at 258 nm. The dashed lines represent the maximum energy available for DPD of these isotopic systems (reproduced by permission of the Royal Society of Chemistry from Reference 71).

for this system because it exhibits constrained, vibrationally adiabatic dissociation dynamics.

These results should provide an important test of both ab initio potential energy surfaces and reaction dynamics calculations for this system. Recent theoretical efforts on simulating the photoelectron spectra and extracting information on the reactive potential energy surfaces in related systems (67, 80–82) will need to be extended to take into account the measurement undertaken here—the coincident measurement of the photoelectron kinetic energy and the photofragment translational energy distributions.

## COINCIDENCE STUDIES OF DISSOCIATIVE PHOTOIONIZATION

Highly differential coincidence measurements of DPI processes are also becoming more routine in recent years. In this review, the primary focus is on DPI of neutral molecules via direct excitation to a repulsive ionic state. These processes lead to one neutral species, one ion, and a free electron. There have also been extensive studies of the dissociation of multiply ionized molecules. In fact, many of the important coincidence techniques used today, such as PEPICO and threshold PEPICO (TPEPICO), were developed and applied to the study of the dissociation dynamics of multiply ionized molecules (36). The current generation of highly differential, energy- and angle-resolved PEPICO experiments use full-solid-angle imaging detectors for high sensitivity and good counting statistics. Similar to the DPD experiments discussed above, important insights can be gained from examining both photoelectron-photoion energy and angular correlations. DPI processes have received considerably more attention as a source of MF-PADs than studies of DPD in anions, as discussed below.

An example of the newest experiments on DPI processes is provided by the study of Lafosse et al (43) on vector correlations in the DPI of NO in the vacuum UV. This experiment, carried out with 22- to 25-eV photons, made use of time- and position-sensitive detection of the full solid angle for both photoelectrons and photoions. In this arrangement, the kinetic energy and recoil angle correlations for the photoproducts (electron and cation) can be recorded, providing characterization of the dissociative electronic states and a direct measure of the MF-PAD. In this study, $NO(X\,^2\Pi)$ was ionized to the dissociative $NO^+(c\,^3\Pi)$ or $NO^+(B\,^1\Pi)$ states, with rapid dissociation to $N^+(^3P) + O(^3P) + e^-$. Measuring the $N^+$ and $e^-$ in coincidence thus gives a kinematically complete characterization of this DPI process.

An example of the energetic correlations seen in such an experiment is shown in Figure 5, where three processes are identified in the two-dimensional histogram of the correlation of the photoelectron and photoion kinetic energy. Processes *I* and *II* both correspond to ground state products $N^+(^3P) + O(^3P) + e^-$, as shown by their position along the energetic limit for this process marked $L_1$. The different photoelectron kinetic energies, however, allow assignment of process *I* to DPI via the $NO^+(c^3\Pi)$ state, whereas process *II* is DPI via the higher lying $NO^+$ $(B\,^1\Pi)$ state. The photoelectron kinetic energy near 0.3 eV identifies process *III* as also occurring via the $NO^+(B\,^1\Pi)$ state. The limits $L_2$ and $L_3$ in this case, however, correspond to excited-state dissociation channels, producing $N^+(^1D)$ or $O(^1D)$ excited products, respectively. This coincidence experiment allows direct determination of the branching ratios between these different channels for the first time. In addition to the energetic correlations, the photoelectron–photoion angular correlations yielded the MF-PAD for feature *I* in the correlation spectrum, providing further insights into the DPI dynamics.

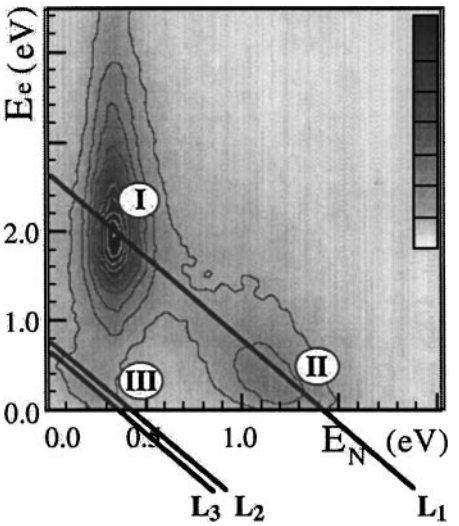


**Figure 5** Photoelectron-photoion kinetic energy correlation diagram for NO + h$\nu$ $\rightarrow$ $N^+ + O + e^-$, where h$\nu$ is 23.6 eV. The limits marked $L_1$, $L_2$, and $L_3$ correspond to the dissociation limits $N^+(^3P) + O(^3P) + e^-$, $N^+(^1D) + O(^3P) + e^-$, and $N^+(^3P) + O(^1D) + e^-$, respectively (reproduced from Reference 43 with permission from the American Physical Society).

When dissociation is rapid relative to molecular rotation, the axial recoil approximation holds, and fully angle-resolved PEPICO experiments directly yield the MF-PAD. Several experiments have probed the MF-PAD in recent years, but now, with high-sensitivity energy- and angle-resolved PEPICO experiments becoming possible, the quality of the measured MF-PADs has improved considerably. In addition to the studies of NO by Lafosse et al (43), recent reports have appeared on the $H_2$ (83), $O_2$ (40, 84), CO (85), $N_2$ (86, 87), and $CO_2$ (86, 87) molecules.

For larger polyatomic molecules, Downie & Powis (42, 88, 89) have reported fully angle-resolved PEPICO studies of $CF_3I$. They examined the photoelectron–photoion recoil vector correlations in the DPI of $CF_3I$ by photoionization of the $5a_1$ valence orbital with 21.2-eV radiation from a He discharge lamp. At this photoionization wavelength, DPI pathways leading to both $CF_3^+ + I(^2P_{1/2}, {}^2P_{3/2})$ and $I^+ + CF_3$ are open. An example of the electron–$CF_3^+$ recoil vector correlations is shown in Figure 6. For valence photoionization, it is expected that examination of the electron-ion vector correlations will give the same results for these two channels if the axial recoil approximation holds, in agreement with the results of Downie & Powis over a wide range of energies. At lower available energies, however, the more endothermic $I^+$ channel shows differences consistent with dynamical effects in this dissociation channel and the breakdown of the axial recoil approximation. Downie & Powis (42) also carried out calculations on the electron-molecule half collision that occurs on photoionization, recovering the major features of the observed MF-PAD for the stable polyatomic molecule, $CF_3I$.

A number of collisional and photoinduced processes involving atoms and, more recently, molecules have been carried out using the cold target recoil ion

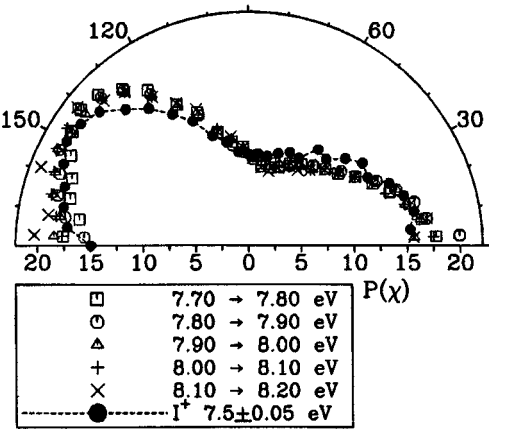


**Figure 6** Polar plot of photoelectron-cation recoil vector correlations over a range of photoelectron kinetic energies. The probability $P(\chi)$ as a function of the included angle $\chi$ between the photoelectron and ion recoil direction in the He(I) DPI of $CF_3I$ is plotted here. The data for $I^+$ (solid circles) is plotted against the conjugate angle $\chi' = 180^\circ - \chi$, so that the direction $\chi = 180^\circ$ always corresponds to ejection of the electron from the I atom end of the molecule (reproduced from Reference 42 with permission from the American Institute of Physics).

momentum spectroscopy (COLTRIMS) technique (41, 90). These experiments are entirely analogous to those already discussed in that the recoil momenta of the products are measured directly to provide a kinematically complete measure of the process under study. An example of the recent extension of these techniques to molecular problems is given by the study of the double ionization of $D_2$ (91). In this experiment, the momenta of both deuterons and one of the two photoelectrons were measured, yielding kinematically complete data on the dynamics of this DPI process. This process provides an important test of electron correlation phenomena because both electrons are removed by a single photon. COLTRIMS experiments have been recently reviewed in detail (90).

## TIME-RESOLVED DYNAMICS—PHOTOELECTRON-PHOTOION ENERGY AND ANGULAR DISTRIBUTIONS: $NO_2$

Advances in ultrafast laser technology coupled with the increasing use of sophisticated time- and position-sensitive detectors have paved the way for carrying out time-resolved coincidence studies on dissociating systems. Hayden and coworkers (30) recently constructed a time-resolved PEPICO spectrometer that allows

complete three-dimensional energy and angular distributions to be collected in coincidence for photoelectrons and photoions. More conventional time-resolved PEPICO experiments by Radloff (18) looked at the time evolution of the photoionization of ammonia clusters, benzene dimers, and other systems in which photoelectron spectra for many different species can be acquired as a function of time using the coincident photoion to sort the results. Gas-phase ultrafast studies can often be challenging because of the propensity for the occurrence of multiphoton processes. Kinematically complete coincidence experiments, like those carried out by Hayden and coworkers (30), can play an important role in ultrafast studies by helping to verify what photoexcitation pathways are operative. As seen in the studies of DPD and DPI reviewed above, a coincidence measurement of the kinetic energies of the photoelectron and the photofragments helps deduce the final states of the products and, when multiphoton processes are possible, determine how many photons are involved.

The first time-resolved coincidence study of photoelectron-photoion kinetic energy partitioning is that of the dissociative multiphoton ionization (DMI) of $NO_2$ at 375 nm reported by Davies et al (30). Previous studies of the DMI of $NO_2$ at this wavelength were interpreted in terms of a one-photon excitation to the lowest dissociative state of $NO_2$, followed by three-photon ionization of the NO products (92). By carrying out a fully energy- and angle-resolved PEPICO experiment, Davies et al (30) were able to show that DMI with 150-fs laser pulses at this wavelength occurs via three-photon excitation to a state of $NO_2$ correlating to the NO($C^2\Pi$)+ O dissociation limit, with ionization of the nascent NO by a fourth photon. Figure 7 shows the time evolution of the photoelectron-photoion kinetic energy correlations observed in this experiment. The photoion kinetic energy axis shows the CM $E_T$ in the dissociation of NO + O that occurs on the excited state of $NO_2$. At short times, a diagonal structure is observed, similar to the DPD of $O_4^-$ and the DPI of NO discussed above. This diagonal structure is a measure of the distribution of the original molecular wave packet over the repulsive state of $NO_2$ that is accessed by three-photon excitation. As the bond breaks, the correlation spectra evolve at longer times to show along the *y*-axis the photoelectron spectrum of NO($C^2\Pi$) and along the *x*-axis the translational energy distribution of the NO($C^2\Pi$) products. The photoelectron–photoion kinetic energy correlations can thus be used to examine the breaking of the O–NO bond over a time scale of a few hundred femtoseconds.

Since the dissociation is so rapid and the experiment records the recoil angles of the coincident photoelectrons and photoions, the DMI of $NO_2$ provides another example of how coincidence experiments can be used to determine the MF-PAD. The results of Davies et al (31) shown in Figure 8 illustrate the time evolution of the MF-PAD during the dissociation. The data shown here represent the angular distribution of the photoelectrons for only the ions that recoil along the electric vector of the laser, and one can see how this evolves from a noncentrosymmetric angular distribution at short times to a centrosymmetric one at long times, as the now free NO rotates away from the recoiling O atom. At short times, as shown

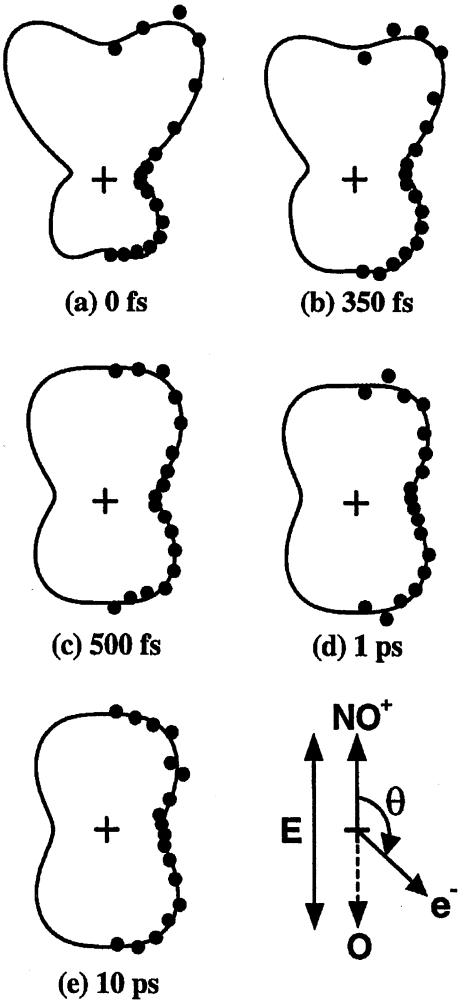


**Figure 8** Time-resolved molecular-frame photoelectron angular distributions for the dissociative multiphoton ionization of $NO_2^-$ at 375.3 nm. The angular distribution (in number of events per unit solid angle) is shown by the distance from the origin as a function of the angle $\theta$ shown in the lower right-hand corner of the figure. The data were recorded with both pump and probe laser polarization parallel and show the angular correlations for ions recoiling along that axis. The solid-line fits represent the best-fit sum of Legendre polynomials (reproduced from Reference 31, with permission from the American Physical Society).

in Figure 8, there is a marked propensity for both the photoelectron and $NO^+$ to recoil in the same direction in the molecular frame, defined by the dissociating bond in $NO_2$.

Qualitatively, the evolution of the angular distributions can be understood in terms of the effect that the close proximity of the recoiling O atom has on the photoelectron. The presence of the neutral O atom causes the interaction potential seen by the departing photoelectron to be highly nonspherical, with a strong inversion asymmetry. The ejected electron scatters from this nonspherical potential, leading to a larger contribution of odd and higher-order partial waves than observed in free $NO(C^2\Pi)$. Quantum interference between these odd and even partial waves can lead to the lobed structure and forward-backward asymmetry seen in these MF-PADs at short time delays. This is similar to previously observed forward-backward asymmetric angular distributions seen in MF-PADs for inner-shell ionization of CO (85) and dissociative autoionization of excited $O_2$ molecules (84).

Quantitative interpretation of these time-dependent results poses a significant challenge for both quantum chemistry and reaction dynamics theory. The dissociation occurs on a highly excited dissociative electronic state of $NO_2$, and detailed prediction of the PADs requires solving the electron-molecule scattering problem for the dissociating $NO_2$. The appearance of experimental observables like this, however, should motivate further studies on the time-resolved properties of PADs.

## THREE-BODY DISSOCIATION DYNAMICS

An increasing number of studies are applying coincidence techniques to the characterization of three-body dissociation dynamics. Important insights into three-body photodissociation processes of stable molecules have been made previously by noncoincidence methods, using measurements of the uncorrelated asymptotic properties of the photofragments, such as momentum and quantum state, to infer the three-body dissociation dynamics (32, 33). Coincidence measurements have the benefit of not requiring significant assumptions about the nature of the dissociation process (concerted/sequential) or geometry at the transition state. The coincidence studies of three-body dissociation reactions allow a direct determination of the product angular correlations and partitioning of momenta, yielding a detailed picture of the dissociation dynamics and even structural insights. Recent experiments on DPD, as well as charge-exchange and collision-induced dissociation studies of three-body dynamics, are reviewed here.

Three-body dissociation processes in molecular physics were first studied using coincidence techniques in Coulomb explosion processes involving multiply ionized molecules. These experiments focused on either multiple photoionization (38, 93) or collisional ionization of a target molecule (37). Such processes have an important advantage for coincidence experiments in that they always produce at least two positively charged fragments that can be detected relatively easily.

Hsieh & Eland (38) and Lavollée (60), for example, have studied the three-body dissociation dynamics of species such as $OCS^{2+}$ and $SO_2{}^{3+}$, respectively. Because two out of the three momenta of the products are all that are required to fully characterize a three-body process, this measurement is sufficient. These measurements, however, are not truly kinematically complete because they do not record the energy of the photoelectrons in the case of photoionization.

PPC experiments provide a new approach to studying three-body dissociation in the ground and low-lying excited states of neutral species. After the development of a new multiparticle detector (34), we applied this technique to the study of the three-body dynamics of $O_6$ (94, 95) and $O_3(D_2O)$ (96) complexes produced upon photodetachment of the corresponding anions. In these studies, multihit time- and position-sensitive particle detectors were used to record the three-dimensional momentum distributions of the photoelectron and three photofragments produced in the DPD of these anions.

PPC studies of three-body dissociation dynamics can be used to study energy partitioning, photoelectron-photofragment angular correlations, and laboratory angular distributions similar to the two-body processes discussed above. For the purpose of this review, the focus is on the vector correlations of the three heavy particles produced in three-body DPD. To directly view the product angular correlations, we follow an approach similar to that used by Hsieh & Eland (38) and Lavollée (60) for the three-body dissociation dynamics of doubly charged cations. Since the three particle recoil velocities are directly measured, once the product masses are determined by evaluating the conservation of momentum, the partitioning of product momenta can be examined.

One of the first systems examined for three-body DPD was the $O_6{}^-$ cluster formed on the addition of an $O_2$ molecule to the $O_4{}^-$ system discussed above. Energy partitioning in the three-body DPD of $O_6{}^-$:

$$O_6{}^- + h\nu \rightarrow O_2 + O_2 + O_2 + e^- \qquad 5.$$

is very similar to that observed for $O_4{}^-$. In particular, vibrationally resolved $N(E_T, eKE)$ correlation spectra are observed (94). A more detailed view into the three-body half-collision dynamics can be seen in the MF-DCS spectra shown in Figure 9*a* for the breakup of $O_6{}^-$ at 388 nm (3.20 eV). In this spectrum, the CM momentum of the fastest particle is constrained to lie along the *x*-axis. On an event-by-event basis, the direction and magnitude of the momentum vectors of the other products are plotted in the plane of the figure. The partitioning of momentum in the DPD of $O_6{}^-$ reveals an anisotropic distribution in which two of the $O_2$ products carry away the majority of the momentum, and the third $O_2$ plays the role of a spectator. These dynamics are consistent with an $O_4{}^-$ core weakly interacting with the third $O_2$. Because of the weakly bound open-shell character of $O_6{}^-$, it is difficult to carry out reliable ab initio calculations to confirm the structure of this system. However, given that $O_6{}^-$ is bound by only $\sim$0.11 eV relative to $O_4{}^-$, a weak electrostatic interaction with the third $O_2$ is very plausible (94).

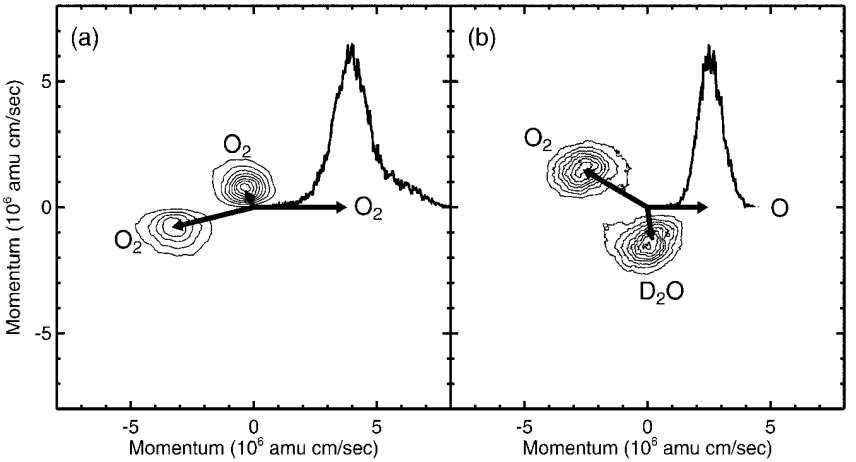


**Figure 9** Momentum-space molecular-frame differential cross section spectra recorded in the three-body dissociative photodetachment of $O_6^-$ (*panel A*) and $O_3^-(D_2O)$ (*panel B*). In *panel A*, the fastest $O_2$ product is chosen as the reference particle along the *x*-axis, whereas in *panel B*, the fastest of the two lighter particles is assigned to be the O atom and chosen as the reference particle as discussed in the text. The vectors show the peaks of the correlated distributions in both frames (adapted from References 95 and 96, by permission. Copyright (2001) American Chemical Society).

The three-body recombination reaction $O + O_2 + M \rightarrow O_3 + M$ is responsible for the formation of stable ground-state $O_3$ in the atmosphere. Therefore, this system is an important prototypical three-body system to study. Photodetachment of $O_3^-(D_2O)$ clusters at 258 nm (4.80 eV) was used to prepare the dissociative low-lying triplet and singlet excited states of $O_3(D_2O)$, following an earlier study of the dissociation dynamics of these states in free $O_3$ (75). Photodetachment to the triplet states of $O_3$ in the complex leads to three-body dissociation as follows:

$$O_3^-(D_2O) + h\nu \rightarrow O + O_2 + D_2O + e^-, \qquad 6.$$

with no evidence observed for intracluster reaction or quenching of the excited states in the complex at the level of excitation used in this experiment (96). Once again, the detailed dynamics of the three-body dissociation of the excited $O_3(D_2O)$ complex can be studied by examining the angular correlations of the product recoil vectors. In this case, the MF-DCS is generated by transforming the data from the laboratory frame to a molecular breakup frame such that for each event, the velocity vector of the O atom is chosen as the principal axis, and the recoil velocities of the other two particles are then plotted in this CM reference frame as shown in Figure 9*b*.

The mass resolution in these experiments is currently limited: $O_2$ can be fully resolved from O and $D_2O$, but the lighter fragments cannot be fully resolved from

one another. Because of this limitation, the assumption is made in generation of the MF-DCS that the O atom is the fastest particle. The MF-DCS shows that the centroid of the $O_2$ distribution recoils backward relative to the O atom, whereas the centroid of the $D_2O$ feature is actually observed to be slightly forward scattered relative to the recoiling O atom. The striking result from the MF-DCS is that the product momenta are partitioned such that the heaviest fragment, $O_2$, carries away most of the momentum, with the lighter O and $D_2O$ fragments recoiling in the other direction in the CM. This observation is not affected by the assumption that the O atom is the fastest product.

To gain further insights into the three-body dissociation dynamics indicated by the MF-DCS, density functional theory calculations of the structure of the parent $O_3^-(D_2O)$ complex were performed. Two nearly isoenergetic local minima were found: an asymmetric $C_s$ complex with $D_2O$ hydrogen bonded to one end of $O_3^-$ and a double-hydrogen-bonded $C_{2v}$ complex. The calculated $C_s$ geometry showed that the O–D bond in the water moiety and the O–$O_2$ bond interacting with the $D_2O$ are both longer than their respective equilibrium bond lengths. This breaking of the $C_{2v}$ symmetry of $O_3$ in the cluster is expected to promote the antisymmetric stretch dissociation of the lengthened O–$O_2$ bond, which has been shown to be the reaction coordinate for dissociation of the low-lying excited states of $O_3$ in previous studies (75).

The asymmetric structure of the cluster is consistent with the observations if the lengthened O–$O_2$ bond breaks, causing the recoiling O atom to interact with $D_2O$, transferring some momentum to the nearly equal mass $D_2O$. The heavier $O_2$ product then carries away the largest fraction of the momentum as it recoils in the other direction. Dissociation of the $C_{2v}$ symmetry complex would not be expected to lead to such a striking partitioning of momentum between the light and heavy fragments. The three-body DPD of $O_6^-$ and $O_3^-(D_2O)$ provides examples of the insights into three-body dissociation dynamics and even the structures of transient neutral species that can be obtained in photoelectron–multiple-photofragment coincidence experiments.

A second type of kinematically complete three-body dissociation experiment on neutral species has been carried out by Müller and coworkers (35), who used the charge-exchange technique to study the three-body breakup of neutral triatomic hydrogen. In this study, specific excited ro-vibronic states of $H_3$ were prepared by laser excitation, taking advantage of the single long-lived rotational state of neutral $H_3$ formed by charge exchange of a 3-keV $H_3^+$ beam with cesium. Using a time- and position-sensitive multiparticle detector to detect the three H atoms in coincidence, they found that the three-body dissociation dynamics exhibit a strong dependence on the initially excited Rydberg states of $H_3$. They also adapted the three-body analysis procedures developed by Dalitz (97) for nuclear scattering studies and applied increasingly to problems in atomic and molecular physics (98). The Dalitz plots show the partitioning of the square of product momenta and provide fundamental insights into the three-body dynamics, similar to the

MF-DCS discussed above. These representations of the three-body dynamics are being used increasingly, as discussed recently by Maul & Gericke (33), and can also be applied to the DPD experiments discussed above.

A final current topic to be reviewed here is the three-body collision-induced dissociation of $Na_n^+$ clusters in collisions with He at energies from 160 to 260 eV. These experiments, carried out by Barat et al (99), use multicoincidence detection of neutral and ionic products to study the three-body dissociation reactions $Na_n^+ \rightarrow Na_{n-2}^+ + Na + Na$, where $n$ is 3, 4, and 5. In these collision-induced dissociation processes, in addition to the individual velocity vectors of the products, it is useful to examine the deflection of the centroid of the three products from the collision with He. This deflection provides a measure of the momentum transfer in the collisions. The dynamics observed for the $Na_3^+$ system are consistent with electronic excitation to a repulsive ionic state with prompt dissociation. In the larger clusters, however, the dominant mechanism involves momentum transfer to the Na atoms in the collision with He with ejection of a fast neutral Na atom, followed by dissociation of the excited ionic fragment. These types of collisions are characterized by one fast neutral product, one slow neutral product, and an ionic product with a momentum matching that of the slow neutral product of the subsequent dissociation of the excited ionic fragment. Kinematically complete coincidence measurements like those reported by Barat et al (99) provide the necessary information to unravel the complicated three-body dissociation dynamics observed in full collisions at high energies.

## CONCLUDING REMARKS

Coincidence spectroscopies will likely play an increasing role in the elucidation of the energetics and reaction dynamics of transient species. Further advances in detection technology and laser and synchrotron excitation sources will provide the required tools. One promising development is the potential for new pixellated detectors that should become available as a spin-off of technology originally developed for particle physics experiments. Research in this area is currently being driven by the need for real-time high-throughput X-ray crystallography applications in biophysics (100). These devices will share many of the characteristics of the current CCDs used in imaging studies in chemical dynamics, but they will have the added benefit of full three-dimensional information: $x$,$y$ position and particle time-of-flight. Of course, the application of detection schemes like this will need to be coupled with improved, higher-speed data acquisition interfaces, which will likely occur.

In conclusion, we have discussed some of the diverse recent applications of coincidence spectroscopic techniques to the study of the energetics, dissociation, and ionization dynamics of isolated molecules and clusters. We have focused on the unique types of information that can be derived from coincidence studies of

these fundamental processes in chemical dynamics, including characterization of dissociative states, regions of potential energy surfaces near the transition state for bimolecular reactions, MF-PADs, and three-body dissociation dynamics.

## ACKNOWLEDGMENTS

I thank the members of my group, past and present, who have contributed to our coincidence studies of DPD processes. Research support from the Air Force Office of Scientific Research, the National Science Foundation, and the U.S. Department of Energy is gratefully acknowledged. REC is a Camille Dreyfus Teacher Scholar and a David and Lucile Packard Fellow in Science and Engineering.



## LITERATURE CITED

1. Butler LJ, Neumark DM. 1996. *J. Phys. Chem.* 100:12801–16
2. Casavecchia P. 2000. *Rep. Prog. Phys.* 63:355–414
3. Mayer PM, Parkinson CJ, Smith DM, Radom L. 1998. *J. Chem. Phys.* 108:604–15
4. Roos BO. 1999. *Acc. Chem. Res.* 32:137–44
5. Palma J, Clary DC. 2000. *J. Chem. Phys.* 112:1859–67

5a. Ng C, ed. 2000. *Photoionization and Photodetachment*, Vol. 10A, B. Singapore: World Scientific

6. Weitzel K-M. 2000. See Ref. 5a, Vol. 10A, pp. 539–600
7. Morioka Y. 2000. See Ref. 5a, Vol. 10A, pp. 347–93
8. Heck AJR, Chandler DW. 1995. *Annu. Rev. Phys. Chem.* 46:335–72
9. Houston PL. 1996. *J. Phys. Chem.* 100:12757–70
10. Parker DH. 2000. See Ref. 5a, Vol. 10A, pp. 3–46
11. Suits AG, Continetti RE. 2001. In *Imaging in Chemical Dynamics*, ed. AG Suits, RE Continetti, *ACS Symp. Ser. 770*. Washington, DC: Am. Chem. Soc.
12. Continetti RE. 2000. See Ref. 5a, Vol. 10B, pp. 748–808
13. Cooper J, Zare RN. 1968. *J. Chem. Phys.* 48:942–45
14. Dill D. 1976. *J. Chem. Phys.* 65:1130–33
15. Park H, Zare RN. 1996. *J. Chem. Phys.* 104:4554–67
16. Zare RN. 1972. *Mol. Photochem.* 4:1–37
17. Hayden CC, Stolow A. 2000. See Ref. 5a, Vol. 10A, pp. 91–126
18. Radloff W. 2000. See Ref. 5a, Vol. 10A: pp. 127–81
19. Cyr DR, Hayden CC. 1996. *J. Chem. Phys.* 104:771–74
20. Wang L, Kohguchi H, Suzuki T. 1999. *Faraday Discuss.* 113:37–46
21. Blanchet V, Zgierski M, Seideman T, Stolow A. 1999. *Nature* 401:52–54
22. Lehr L, Zanni MT, Frischkorn C, Weinkauf R, Neumark DM. 1999. *Science* 284:635–38
23. Seideman T. 1997. *J. Chem. Phys.* 107:7859–68
24. Althorpe SC, Seideman T. 1999. *J. Chem. Phys.* 110:147–55
25. Seideman T. 2000. *J. Chem. Phys.* 113:1677–80
26. Reid KL, Underwood JG. 2000. *J. Chem. Phys.* 112:3643–49
27. Underwood JG, Reid KL. 2000. *J. Chem. Phys.* 113:1067–74
28. Arasaki Y, Takatsuka K, Wang K, McKoy V. 2000. *J. Chem. Phys.* 112:8871–84
29. Reid KL, Field TA, Towrie M, Matousek P. 1999. *J. Chem. Phys.* 111:1438–45

30. Davies JA, LeClaire JE, Continetti RE, Hayden CC. 1999. *J. Chem. Phys.* 111:1–4
31. Davies JA, Continetti RE, Chandler DW, Hayden CC. 2000. *Phys. Rev. Lett.* 84:5983–86
32. Maul C, Gericke KH. 1997. *Int. Rev. Phys. Chem.* 16:1–79
33. Maul C, Gericke KH. 2000. *J. Phys. Chem. A* 104:2531–41
34. Hanold KA, Luong AK, Clements TG, Continetti RE. 1999. *Rev. Sci. Instrum.* 70:2268–76
35. Müller U, Eckert T, Braun M, Helm H. 1999. *Phys. Rev. Lett.* 83:2718–21
36. Eland JHD. 1991. In *VUV Photoionization and Photodissociation of Molecules and Clusters*, pp. 297–343. Singapore: World Sci.
37. Werner U, Beckord K, Becker J, Lutz HO. 1995. *Phys. Rev. Lett.* 74:1962–65
38. Hsieh S, Eland JHD. 1997. *J. Phys. B* 30:4515–34
39. Stert V, Radloff W, Schulz CP, Hertel IV. 1999. *Eur. Phys. J. D* 5:97–106
40. Takahashi M, Cave JP, Eland JHD. 2000. *Rev. Sci. Instrum.* 71:1337–44
41. Doerner R, Mergel V, Spielberger L, Achler M, Khayyat K, et al. 1997. *Nucl. Instrum. Methods B* 24:225–31
42. Downie P, Powis I. 1999. *J. Chem. Phys.* 111:4535–47
43. Lafosse A, Lebech M, Brenot JC, Guyon PM, Jagutzki O, et al. 2000. *Phys. Rev. Lett.* 84:5987–90
44. Wiza JL. 1979. *Nucl. Instrum. Methods* 162:587–601
45. DeBruijn DP, Los J. 1982. *Rev. Sci. Instrum.* 53:1020–26
46. van der Zande WJ, Koot W, Los J. 1989. *J. Chem. Phys.* 91:4597–602
47. Beijersbergen JHM, van der Zande WJ, Kistemaker PG, Los J, Drewello T, Nibbering NMM. 1992. *J. Phys. Chem.* 96:9288–93
48. Helm H, Walter CW. 1993. *J. Chem. Phys.* 98:5444–49
49. Helm H, Cosby PC. 1987. *J. Chem. Phys.* 86:6813–22
50. Continetti RE, Cyr DR, Osborn DL, Leahy DJ, Neumark DM. 1993. *J. Chem. Phys.* 99:2616–31
51. Bise RT, Choi H, Neumark DM. 1999. *J. Chem. Phys.* 111:4923–32
52. Hanold KA, Sherwood CR, Garner MC, Continetti RE. 1995. *Rev. Sci. Instrum.* 66:5507–11
53. Deyerl H-J, Alconcel LS, Continetti RE. 2001. *J. Phys. Chem.* In press
54. Martin C, Jelinsky P, Lampton M, Malina RF, Anger HO. 1981. *Rev. Sci. Instrum.* 52:1067–74
55. Brenot J-C, Durup-Ferguson M. 1992. *Adv. Chem. Phys.* 82:309–99
56. Belkacem A, Faibis A, Kanter EP, Koenig W, Mitchell RE, et al. 1990. *Rev. Sci. Instrum.* 61:945–52
57. Levin J, Feldman H, Baer A, Ben-Hamu D, Heber O, et al. 1998. *Phys. Rev. Lett.* 81:3347–50
58. Amitay Z, Zajfman D. 1997. *Rev. Sci. Instrum.* 68:1387–92
59. Ali I, Dorner R, Jagutzki O, Nuttgens S, Mergel V, et al. 1999. *Nucl. Instrum. Methods B* 149:490–500
60. Lavollée M. 1999. *Rev. Sci. Instrum.* 70:2968–74
61. Wenthold P, Hrovat DA, Borden WT, Lineberger WC. 1996. *Science* 272:1456–59
62. Metz RB, Bradforth SE, Neumark DM. 1992. *Adv. Chem. Phys.* 81:1–61
63. Manolopoulos DE, Stark K, Werner H-J, Arnold DW, Bradforth SE, Neumark DM. 1993. *Science* 262:1852–55
64. de Beer E, Kim EH, Neumark DM, Gunion RF, Lineberger WC. 1995. *J. Chem. Phys.* 99:13627–36
65. Arnold DW, Cangshan X, Neumark DM. 1995. *J. Chem. Phys.* 102:6088–99
66. Thompson WH, Miller WH. 1994. *J. Chem. Phys.* 101:8620–27
67. Clary DC, Gregory JK, Jordan MJT, Kauppi E. 1997. *J. Chem. Soc. Faraday Trans.* 93:747–53

68. Hanold KA, Sherwood CR, Continetti RE. 1995. *J. Chem. Phys.* 103:9876–79
69. Hanold KA, Garner MC, Continetti RE. 1996. *Phys. Rev. Lett.* 77:3335–38
70. Hanold KA, Continetti RE. 1998. *Chem. Phys.* 239:493–509
71. Deyerl H-J, Luong AK, Clements TG, Continetti RE. 2000. *Faraday Discuss. Chem. Soc.* 115:147–60
72. Sherwood CR, Hanold KA, Garner MC, Strong KM, Continetti RE. 1996. *J. Chem. Phys.* 105:10803–11
73. Posey LA, Deluca MJ, Johnson MA. 1986. *Chem. Phys. Lett.* 131:170–74
74. Aquino A, Walch S, Taylor PR. 2000. *J. Chem. Phys.* 114:3010–17
75. Garner MC, Hanold KA, Resat MS, Continetti RE. 1997. *J. Phys. Chem. A* 101:6577–82
76. Resat MS, Zengin V, Garner MC, Continetti RE. 1998. *J. Phys. Chem.* 102:1719–24
77. Sherwood CR, Garner MC, Hanold KA, Strong KM, Continetti RE. 1995. *J. Chem. Phys.* 102:6949–52
78. Reed KJ, Zimmerman AH, Andersen HC, Brauman JI. 1976. *J. Chem. Phys.* 64:1368–75
79. Gygax R, McPeters HL, Brauman JI. 1979. *J. Am. Chem. Soc.* 101:2567–70
80. Thompson WH. 1999. *J. Phys. Chem. A* 103:9500–5
81. Thompson WH. 1999. *J. Phys. Chem. A* 103:9506–11
82. Lavender HB, McCoy AB. 2000. *J. Phys. Chem. A* 104:644–51
83. Ito K, Adachi J, Hall R, Motoki SES, Soejima K, Yagishita A. 2000. *J. Phys. B* 33:527–33
84. Golovin AV, Heiser F, Quayle CJK, Morin P, Simon M, et al. 1997. *Phys. Rev. Lett.* 79:4554–57
85. Heiser F, Gessner O, Viefhaus J, Wieliczek K, Hentges R, Becker U. 1997. *Phys. Rev. Lett.* 79:2435–37
86. Shigemasa E, Adachi J, Oura M, Yagishita A. 1995. *Phys. Rev. Lett.* 74:359–62
87. Pavylchev AA, Fominykh NG, Watanabe N, Soejima K, Shigemasa E, Yagishita A. 1998. *Phys. Rev. Lett.* 81:3623–26
88. Downie P, Powis I. 1999. *Phys. Rev. Lett.* 82:2864–67
89. Downie P, Powis I. 2000. *Faraday Discuss. Chem. Soc.* 115:103–17
90. Doerner R, Mergel V, Jagutzki O, Spielberger L, Ullrich J, et al. 2000. *Phys. Rep.* 330:95–192
91. Doerner R, Brauning H, Jagutzki O, Mergel V, Achler M, et al. 1998. *Phys. Rev. Lett.* 81:5776–79
92. Singhal RP, Kilic HS, Ledingham KWD, Kosmidis C, McCanny T, et al. 1996. *Chem. Phys. Lett.* 253:81–86
93. Lavollée M, Brems V. 1999. *J. Chem. Phys.* 110:918–26
94. Hanold KA, Luong AK, Continetti RE. 1998. *J. Chem. Phys.* 109:9215–18
95. Luong AK, Clements TG, Continetti RE. 2000. See Ref. 11, pp. 313–25
96. Luong AK, Clements TG, Continetti RE. 1999. *J. Phys. Chem. A* 103:10237–43
97. Dalitz RH. 1953. *Philos. Mag.* 44:1068–80
98. Wiese LM, Yenen O, Thaden B, Jaecks DH. 1997. *Phys. Rev. Lett.* 79:4982–85
99. Barat M, Brenot JC, Dunet H, Fayeton JA, Picard YJ. 2000. *J. Chem. Phys.* 113:1061–66
100. Datte P, Beuville E, Beche JF, Cork C, Earnest T, et al. 1997. *Nucl. Instrum. Methods A* 391:471–80

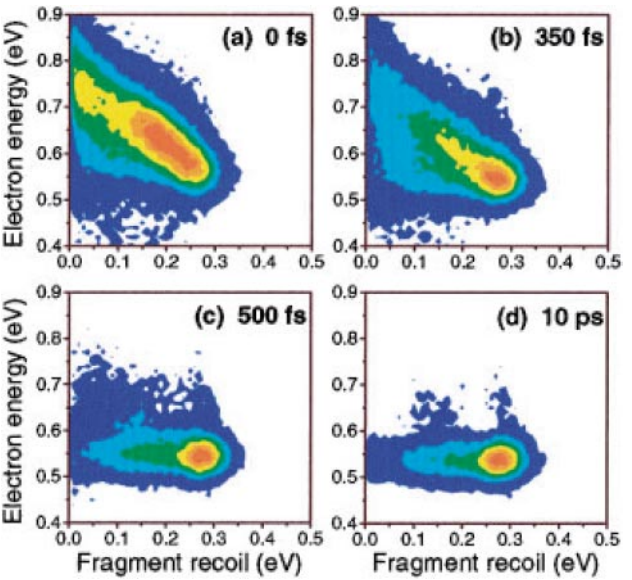


**Figure 7** Time-resolved photoelectron-photoion kinetic energy correlation spectra for the DMI of $NO_2^-$ at 375.3 nm. The number of events are plotted on a linear false-color scale with red representing the peak of the distribution. Reproduced from [Davies, 1999 (30)] with permission from the American Institute of Physics.